

Preventing subsoil enhanced nitrification to safeguard agroecosystem sustainability

Received: 6 January 2026

Accepted: 24 February 2026

Published online: 07 March 2026

 Check for updates

Yao Wang ^{1,2}, Xin Luo ^{2,3} ✉, Esteban G. Jobbágy ⁴, Nandita B. Basu ^{5,6}, Ganlin Zhang ^{7,8}, Yi Zheng ⁹, Baojing Gu ¹⁰, Shaoliang Zhang ¹¹, Yiqi Yu¹, Fenfang Wang¹, Zeyang Lu¹, Ruifeng Yan¹, Scott X. Chang ¹², Yonglong Lu¹ & Nengwang Chen ¹ ✉

The excessive application of nitrogen fertilizers in croplands drives nitrification-induced nitrogen losses, accelerating soil degradation and groundwater nitrate pollution. By synthesizing global nitrogen profiles and field studies, we identify a previously overlooked “enhanced nitrification layer (ENL)” at approximately 0.6 m depth (ranging from 0.3 to 0.9 m) across global croplands. The formation of the ENL relies on the interplay of four key processes: root-mediated nitrogen transport (the conveyor belt), an oxygenated microenvironment sustained by soil texture (the reaction chamber), nitrifier communities (the nitrification engine), and favorable hydrological conditions (the activating switch). This ENL acts as a biogeochemical hotspot, driving subsoil pH declines and nitrate leaching to groundwater. Its identification establishes a precise subsurface target, expanding nitrogen management to address the critical depth of peak transformation alongside surface measures, thereby advancing agroecosystem sustainability.

The overuse of nitrogen (N) fertilizers in croplands has been a global concern for decades^{1–3} with losses still exceeding recovery in harvested materials (global N use efficiency of 55%)⁴. A large amount of non-harvested N is thought to be redistributed and resides in earth critical zones (CZs)^{5–8}, a vital thin skin of the planet open to the complex interactions among air, plants and other organisms, water in the saturated zone, and solid minerals in soils to bedrock^{9,10}. These excess N fertilizers (approximately 90% applied in their reduced form such as ammonium N, i.e., NH₄⁺-N) applied to croplands alter the global N cycle^{11–13}, leading to a series of environmental problems, including soil acidification¹⁴, water quality degradation¹⁵, formation of harmful algal

blooms^{16,17} and hypoxic water zones¹⁸, and increased emissions of greenhouse gases to the atmosphere^{19–21}. The CZs are vital in processing and attenuating N overloads in global croplands yet, to date, out of a total of 257 global critical zone observatories (CZOs), only ~30% of them were explicitly stated to be established in or near croplands (Supplementary Fig. 1 and Supplementary Table 1), with even fewer examining how the structure of cropland CZs regulates the productive use of N fertilizers⁸. Particularly, vertical nitrification patterns resulting from the magnitude and vertical location of N fertilizer transformation zones may be valuable indicators of the capacity of the croplands CZs regulating these overloads at both local and global scales^{22,23}.

¹Fujian Provincial Key Laboratory for Coastal Ecology and Environmental Studies, State Key Laboratory of Marine Environmental Science, College of the Environment and Ecology, Xiamen University, Xiamen, China. ²Laboratory for Sea Space Agent, Department of Earth and Planetary Sciences, The University of Hong Kong, Hong Kong, China. ³Shenzhen Research Institute (SRI), The University of Hong Kong, Shenzhen, China. ⁴Grupo de Estudios Ambientales, CONICET, San Luis, Argentina. ⁵Department of Earth and Environmental Sciences, University of Waterloo, Waterloo, Ontario, Canada. ⁶Water Institute, University of Waterloo, Waterloo, Ontario, Canada. ⁷State Key Laboratory of Soil and Sustainable Agriculture, Institute of Soil Science, Chinese Academy of Sciences, Nanjing, China. ⁸Key Laboratory of Watershed Geographic Sciences, Nanjing Institute of Geography and Limnology, Chinese Academy of Sciences, Nanjing, China. ⁹School of Environmental Science and Engineering, Southern University of Science and Technology, Shenzhen, China. ¹⁰College of Environmental and Resource Sciences, Zhejiang University, Hangzhou, China. ¹¹College of Resources and Environment, Northeast Agricultural University, Harbin, China. ¹²Department of Renewable Resources, University of Alberta, Edmonton, Alberta, Canada. ✉e-mail: xinluo@hku.hk; nwchen@xmu.edu.cn

Nitrification has heterotrophic and autotrophic pathways^{13,24}, with the primary substrates being $\text{NH}_4^+\text{-N}$ and organic N, and the primary product being nitrate N ($\text{NO}_3^-\text{-N}$)²³. In non-cropland ecosystems, heterotrophic nitrification predominates and is tightly coupled to the soil total N (TN, primarily as organic N)^{22,24}. We demonstrate that soil TN exhibits an exponential decline with depth across global non-cropland ecosystems (Fig. 1a, b). This gradient dictates a parallel decrease in nitrification rates, a pattern well-established by site-level studies^{25–28}. In croplands, however, excessive N fertilizer inputs shift the process to autotrophic dominance^{13,22}. Our synthesis of global cropland profiles reveals a stable deviation: a persistent TN bulge at approximately 0.6 m soil depth across time ($p < 0.001$) and strongly related to historical N input ($p < 0.01$) (Fig. 1a, c, d, e). Given the classical exponential

decay of soil organic carbon (Supplementary Fig. 2), this TN bulge signals a profound N-transformation driven by inorganic fertilizers rather than by the mineralization of soil organic components. The shallow bulge's position is well above the peak global water table depth (WTD, 2–7 m), within an oxygenated zone that is optimal for nitrification^{29,30}. We therefore propose that this feature constitutes a previously overlooked Enhanced Nitrification Layer (ENL). This ENL could function as a biogeochemical engine, converting subsurface $\text{NH}_4^+\text{-N}$ into mobile $\text{NO}_3^-\text{-N}$, thereby not only sustaining the observed TN bulge but also directly driving the soil acidification that reduces crop yield and the $\text{NO}_3^-\text{-N}$ leaching that pollutes groundwater, both processes that undermine agroecosystem sustainability. The identification of this ENL thereby serves as a precise and manageable

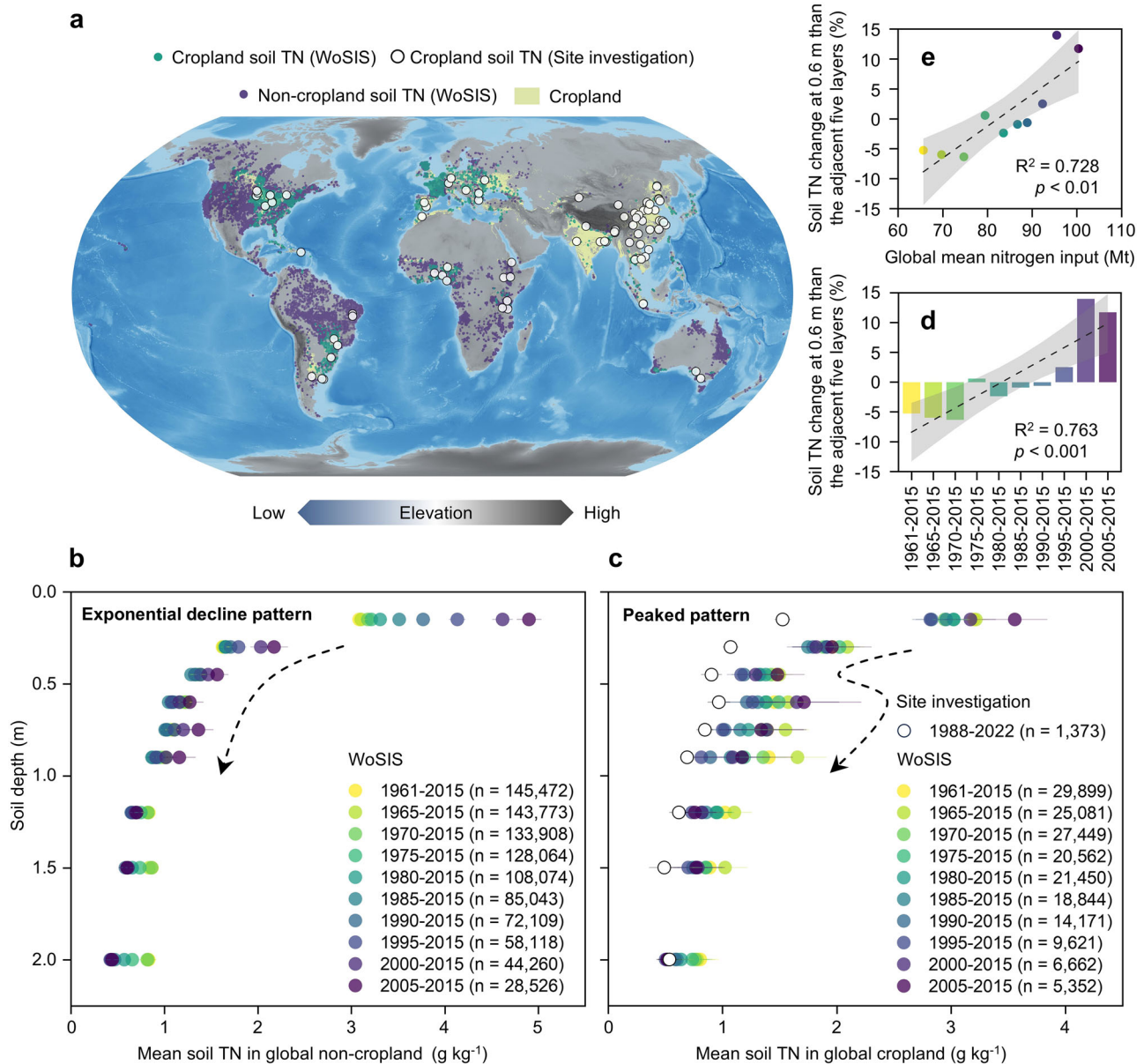


Fig. 1 | Vertical patterns of soil total nitrogen (TN) in global croplands and non-croplands. **a** Site distribution of soil TN in both global croplands and non-croplands. Global soil TN data are obtained from the existing database of the World Soil Information Service (WoSIS) and extensively compiled from the site-level investigations of croplands in the literature (Supplementary Tables 6 and 7). Sites from the WoSIS are classified into cropland and non-cropland types based on the global distribution of land uses at different periods (see Methods). **b, c** The

exponential decline and peak patterns of soil TN in global non-croplands and croplands, respectively. The data are shown with a mean \pm 95% confidence interval. **d, e** Soil TN change at 0.6 m depth compared to the mean of the adjacent five soil layers (the main subsoil depths within 1 m where nitrification occurs, based on refs. 48–51) across time, as well as its relationship with global mean nitrogen input, respectively.

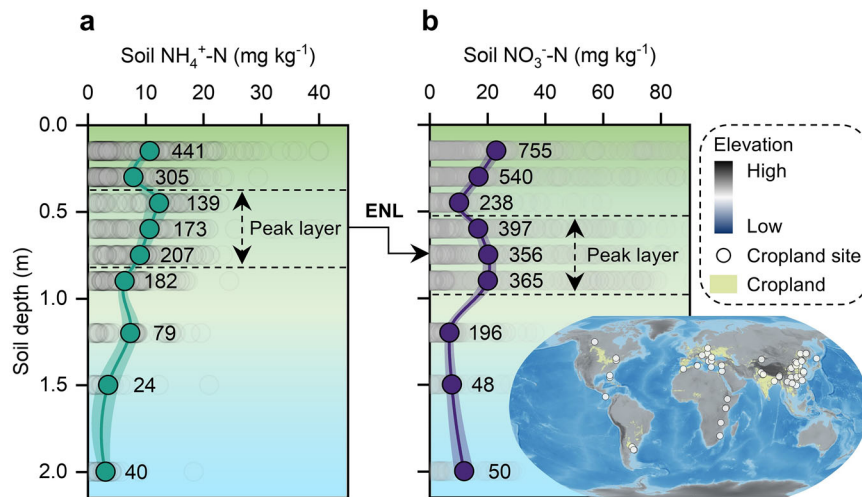


Fig. 2 | Vertical patterns of soil inorganic nitrogen in global croplands. a, **b** Vertical profiles of soil ammonia nitrogen ($\text{NH}_4^+\text{-N}$, nitrification substrate) and nitrate nitrogen ($\text{NO}_3^-\text{-N}$, nitrification product) in global croplands, respectively. The coloured dot line represents the mean values ($\pm 95\%$ confidence interval) at each soil depth, with the adjacent numbers indicating the sample sizes. The gray

dots represent the distribution of the sample values at varying depths. The site locations of soil $\text{NH}_4^+\text{-N}$ and $\text{NO}_3^-\text{-N}$ in global croplands are presented in the world map at the lower right corner. Soil $\text{NH}_4^+\text{-N}$ and $\text{NO}_3^-\text{-N}$ of varying depths are compiled from literature and are detailed in Supplementary Tables 6 and 7. ENL denotes the enhanced nitrification layer.

subsurface target, expanding the paradigm for sustainable N management to integrate the critical depth of peak transformation alongside surface measures.

Results and discussion

Potential location of cropland ENL

Given the scarcity of direct vertical nitrification rate measurements in previous studies, which predominantly focus on surface soils^{22,23}, we thus inferred the potential depth of the ENL from the vertical distributions of nitrification primary substrate ($\text{NH}_4^+\text{-N}$, $n=1590$) and product ($\text{NO}_3^-\text{-N}$, $n=2945$) in global croplands (Fig. 2). Our analysis revealed a distinct subsurface peak in soil $\text{NH}_4^+\text{-N}$ at 0.30–0.75 m depth, whereas the peak soil $\text{NO}_3^-\text{-N}$ occurred deeper at 0.45–0.90 m. The results are highly consistent across different climate zones (Supplementary Fig. 3). Low inorganic N concentrations in the upper layers reflect N transformations and crop uptake in the root zone¹², which together deplete upper soil $\text{NH}_4^+\text{-N}$ and $\text{NO}_3^-\text{-N}$ pools and amplify the relative prominence of the subsurface peaks. This spatial disconnect, with the $\text{NH}_4^+\text{-N}$ peak consistently above the $\text{NO}_3^-\text{-N}$ peak, suggests that while some downward movement of upper-formed $\text{NO}_3^-\text{-N}$ inevitably contributes to subsurface $\text{NO}_3^-\text{-N}$ pools, the observed depth offset requires an additional source of nitrate at depth, most plausibly in-situ nitrification converting $\text{NH}_4^+\text{-N}$ to $\text{NO}_3^-\text{-N}$ along the flow path^{29,31}. Critically, the averaged bulges of nitrification products $\text{NO}_3^-\text{-N}$ were found to be twice as high as the averaged nitrification substrate $\text{NH}_4^+\text{-N}$, although fertilization in croplands predominantly takes the form of $\text{NH}_4^+\text{-N}$ ¹². This disproportionate accumulation of product relative to substrate cannot be explained by leaching alone, which would redistribute rather than amplify $\text{NO}_3^-\text{-N}$. Instead, it points to active N transformation at a specific depth. The inference is further supported by the consistency of these patterns with established correlations between nitrification rates and substrate ($R^2=0.15$, $p<0.001$) and product ($R^2=0.32$, $p<0.001$) pools in global croplands²². We, therefore, infer that the ENL represents a subsurface depth interval (0.3–0.9 m) between these inorganic N peaks, where nitrification activity is enhanced relative to adjacent soil layers. Within this interval, approximately 0.6 m serves as a global reference point that coincides with the persistent TN bulge (Fig. 1c), providing a consistent basis for linking subsurface nitrification to long-term N accumulation across croplands.

Subsurface drives of ENL formation

Having delineated the potential depth of the cropland ENL, we further evaluated whether subsurface conditions could support active nitrification at this horizon. Nitrification process is usually regulated by substrate availability, oxygen content, and the abundance of nitrifiers under favorable hydrological conditions^{22,23,29}. We thus examined these key attributes in the cropland subsurface, namely root extension and decomposition (indicating substrate conveyor and supply), soil texture (influencing oxygen supply), and nitrifying microbe abundance (constituting the nitrification engine), which can modulate the key conditions of nitrification.

First, root extension and subsequent decomposition create voids and channels above the WTD, and facilitate the transfer of nutrients downward from the topsoil³². Thus, we used the maximum rooting depth (MRD), a proxy of root extension for crops, as the attribute to determine the $\text{NH}_4^+\text{-N}$ supply to the ENL. We analyzed the MRD of global plants ($n=2603$) and found that it predominantly falls within the subsoils of 0.6–0.8 m depth (Supplementary Fig. 4), closely aligning with the depth of the ENL and TN bulge. Further supporting this connection, comparative analysis of soil $\text{NH}_4^+\text{-N}$ profiles reveals that deep-rooted crops (primarily fruit and tea trees) exhibit significantly deeper $\text{NH}_4^+\text{-N}$ accumulation peaks than shallow-rooted species (primarily cereals and vegetables) (Fig. 3). These findings indicate that root channels facilitate the vertical transport of applied fertilizers into the ENL³², while simultaneous decomposition of root debris and exudates contributes additional $\text{NH}_4^+\text{-N}$ ³³. Together, these root-mediated processes sustain the substrate supply required to maintain enhanced nitrification within the ENL.

Second, soil texture creates an oxygenated microenvironment³⁴ that supports nitrification within the ENL. We analyzed sand content as a proxy for soil porosity and observed a relatively high sand layer that showed a consistent increase in sand content from 0.45 m depth downward until the 1.2 m depth (Fig. 3). This phenomenon is consistent across different climate zones, except in arid areas (Supplementary Fig. 5). Further supporting this, decadal soil moisture data reveal a distinct relatively dry layer within the ENL depth range (Supplementary Fig. 6). This soil moisture pattern is likely driven by the relatively high sand content in this layer (low water-holding capacity), coupled with root uptake, water table fluctuations, agricultural drainage practices, and anthropogenic climate change^{30,35–38}. Especially

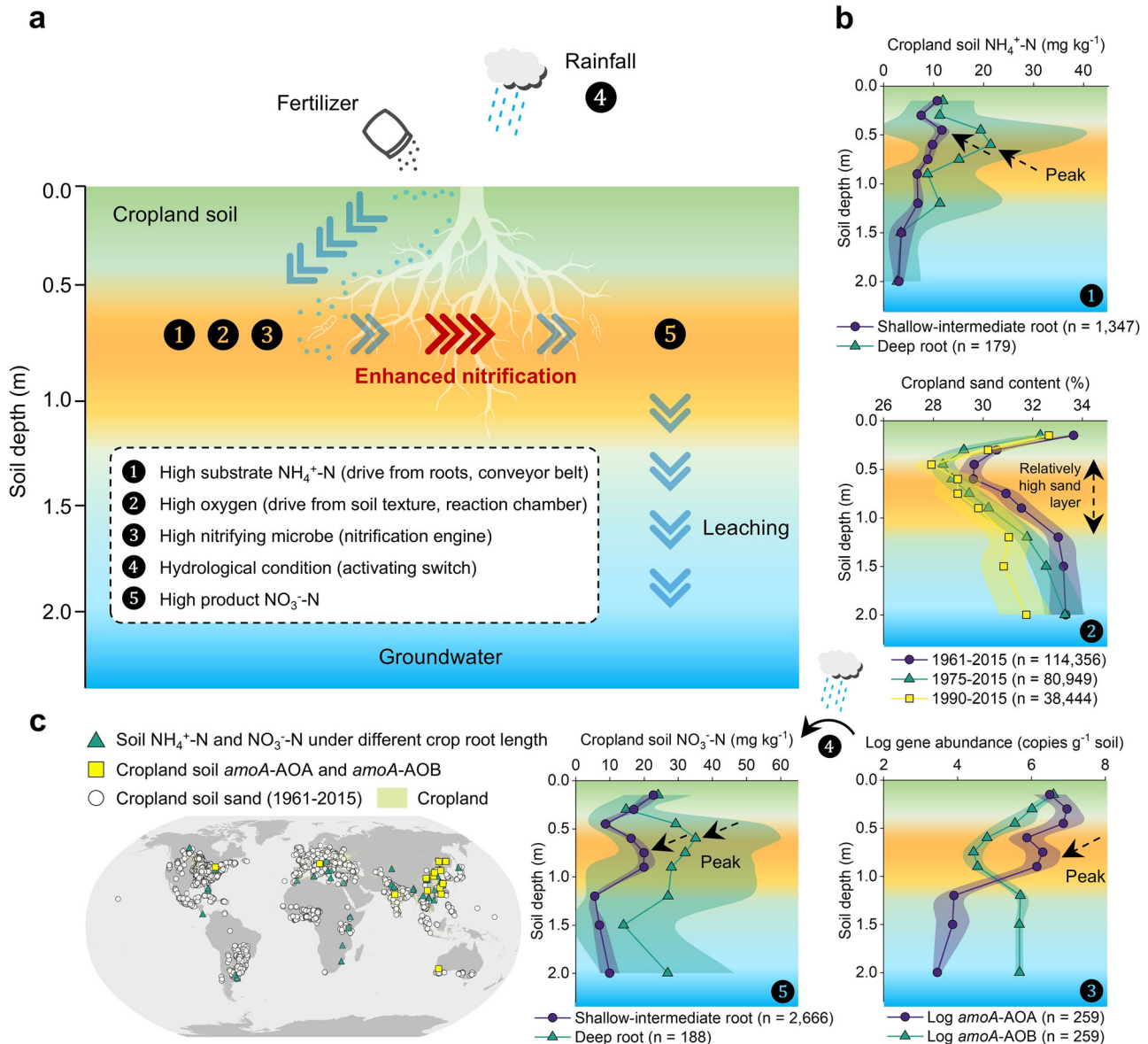


Fig. 3 | Formation mechanism of the Enhanced Nitrification Layer (ENL) in global croplands. **a, b** Conceptual and data-based views of the ENL formation mechanism, respectively. In **a** and **b**, subfigures 1 to 4 represent the four attributes in the formation of ENL, and subfigure 5 shows how ENL leads to elevated nitrate nitrogen (NO_3^- -N). The data are shown with a mean \pm 95% confidence interval. The data on soil ammonium nitrogen (NH_4^+ -N), nitrifying microbes, and soil NO_3^- -N in global croplands are extensively compiled from the literature and can be found in

Supplementary Tables 6 and 7. The data on soil sand content in croplands are extracted from the World Soil Information Service (WoSIS) database based on the global distribution of land uses at different periods (see Methods). **c** Site locations of data used in subfigures 1-3 and 5 of **b**. Subfigure 4 regarding rainfall-activated substrate transport and ENL formation can be found in Fig. 4 and Supplementary Fig. 13. The *amoA*-AOA and *amoA*-AOB represent the ammonia-oxidizing archaea and ammonia-oxidizing bacteria, respectively.

under the future scenario, the subsoil drought (28–100 cm) will continue to increase³⁶. The co-occurrence of elevated sand content and reduced soil moisture within the ENL implies enhanced oxygen availability, thereby fostering favorable conditions for nitrification.

Third, nitrifying microorganisms actively colonize the ENL, providing the biological capacity for enhanced ammonium oxidation²⁹. Our analysis of global nitrifying functional gene profiles ($n = 259$) shows that ammonia-oxidizing archaea (*amoA*-AOA) are present throughout the ENL depth interval (0.3–0.9 m), with highest abundances in the root zone (approximately 0.4 m) and a distinct secondary enrichment at approximately 0.6 m depth (Fig. 3). Sensitivity analysis excluding paddy systems confirms this pattern, showing that the mean *amoA*-AOA abundance at approximately 0.6 m remains elevated, despite wider confidence intervals reflecting greater subsurface

heterogeneity (Supplementary Fig. 7). This consistency confirms that the ENL represents a robust subsurface feature independent of potential confounding effects from flooded systems. These *amoA*-AOA can acclimate to low pH and soil NH_4^+ -N levels, and drive nitrification in a wide range of acidic cultivated soils³⁹. The elevated abundance of these specialized nitrifiers provides a biological basis for the enhanced nitrification activity observed in this subsurface layer.

Case studies for ENL formation

The intrinsic drivers of ENL formation were explored through the comprehensive analysis of subsurface environments in global croplands. However, verifying these mechanisms required field investigations at the CZO scale. To this end, we performed a 3-year measurement on N-components in different CZ sections (regolith and

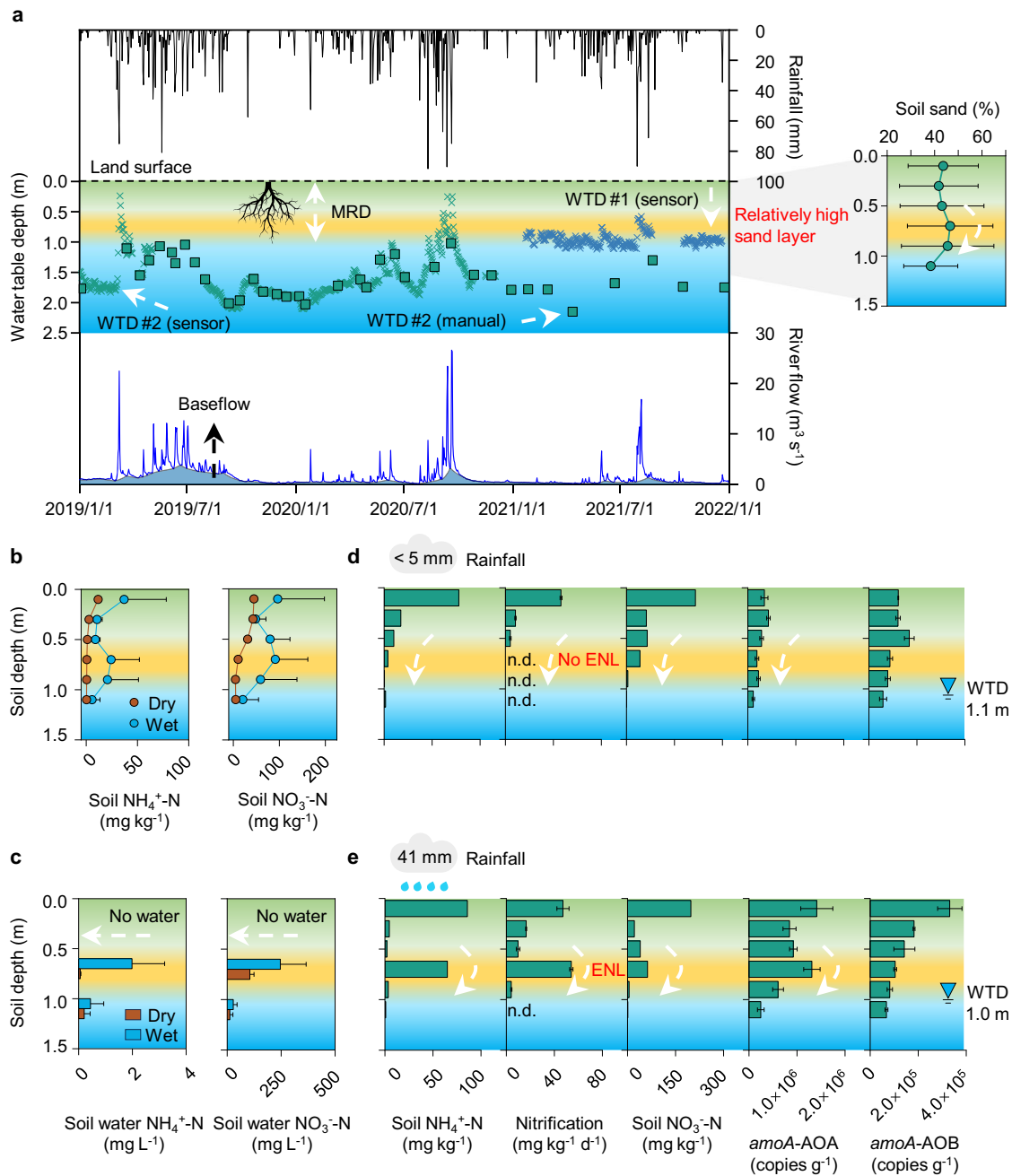


Fig. 4 | Comprehensive observations in the Fengpu stream watershed critical zone observatory (FSW-CZO), southeastern China. **a** The position of the relatively high sand layer, the maximum rooting depth (MRD), and the dynamic changes of regional rainfall, water table depth (WTD), river flow, and baseflow at a daily scale in the FSW-CZO. A detailed FSW-CZO overview can be found in Supplementary Fig. 8. Field images for the distribution of crop roots and WTD in the FSW-CZO can be found in Supplementary Fig. 10. **b, c** Vertical changes of soil and

soil water nitrogen at a seasonal scale, respectively. **d, e** Vertical changes of soil nitrogen, nitrification rate, and gene abundance after two rainfall events in the FSW-CZO. Rainfall indicates the total rainfall during the 20 days before sampling. WTD was recorded on the day of sampling. The *amoA*-AOA and *amoA*-AOB represent the gene abundance of ammonia-oxidising archaea and ammonia-oxidising bacteria, respectively. n.d. denotes not detected. ENL denotes the enhanced nitrification layer.

saturated sections) in the Fengpu Stream Watershed (FSW) CZO, an agricultural system characterized by high fertilizer inputs (Supplementary Figs. 8–12 and Supplementary Tables 2–5).

Integrated analysis of the FSW-CZO identified two key subsurface characteristics: (1) an MRD of 0.6–0.8 m (Fig. 4a and Supplementary Fig. 10), and (2) a relatively high sand layer (0.6–0.8 m) positioned above the WTD fluctuation, as evidenced by high-resolution (daily) and monthly WTD monitoring, together with soil texture investigation (Fig. 4a and Supplementary Table 2). These structural characteristics

closely align with the depth of the global ENL. In particular, elevated $\text{NH}_4^+\text{-N}$ and $\text{NO}_3^-\text{-N}$ in both soil and soil water within the ENL during wet seasons (Fig. 4b, c) suggest that soil N is effectively transported to the relatively high sand layer (ENL depth) through root-mediated pathways under rainfall infiltration, where it undergoes nitrification. Conversely, exponential declines of $\text{NH}_4^+\text{-N}$ and $\text{NO}_3^-\text{-N}$ above WTD during dry seasons indicate that soil $\text{NH}_4^+\text{-N}$ derived from fertilizer and organic matter mineralization is not effectively loaded into the ENL to fuel nitrification. These patterns are consistent with the first ENL

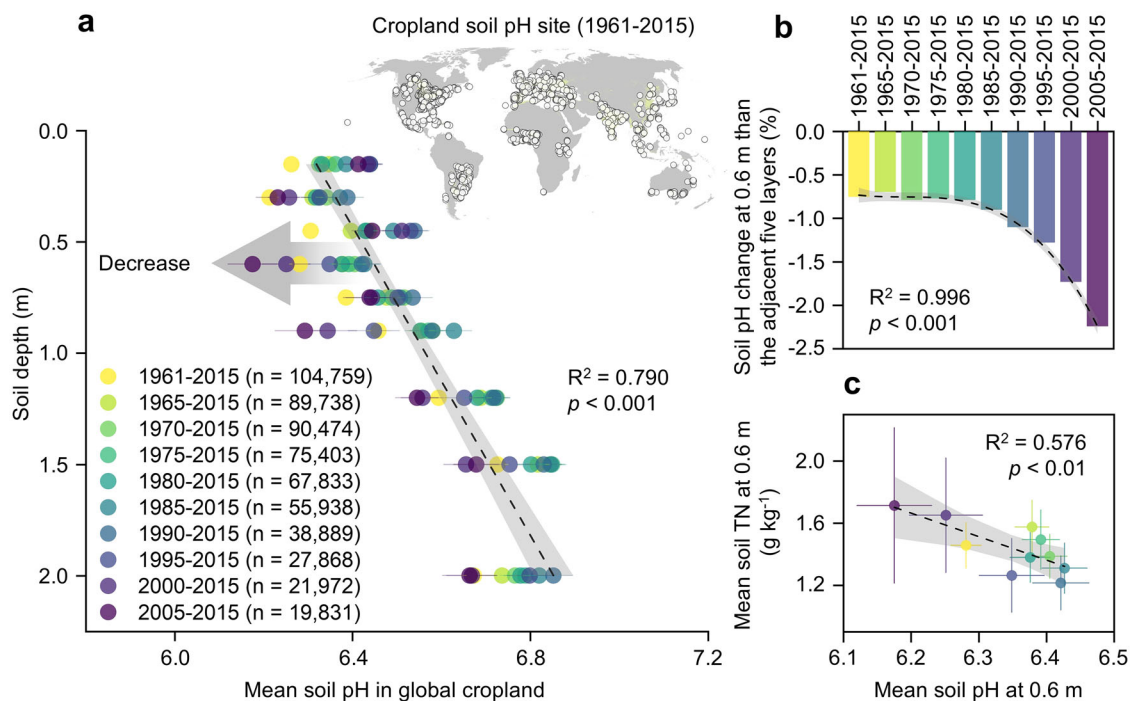


Fig. 5 | Cropland soil pH declines at the depth of the enhanced nitrification layer. **a** Vertical patterns of soil pH in global croplands at different periods. The data are shown with a mean \pm 95% confidence interval. The data on soil pH in croplands are extracted from the World Soil Information Service (WoSIS) database based on the global distribution of croplands at different periods (see

Methods). The site locations of soil pH (1961–2015) in global croplands are presented in the world map at the top right corner. **b** Soil pH changes at 0.6 m depth compared to the mean of the adjacent five soil layers (the main subsoil depths within 1 m where nitrification occurs, based on refs. 48–51) over time. **c** The relationship between soil pH and soil TN at 0.6 m depth.

formation attribute (root-mediated substrate transport) and the second attribute (oxygenated microenvironments maintained by soil texture), while highlighting the importance of hydrological controls.

We further examined how rainfall intensity regulates ENL activation. Following light rainfall, soil N components, nitrification rates, and *amoA*-AOA abundance all exhibited exponential declines with depth (Fig. 4d, e). In contrast, heavy rainfall events triggered substantial increases in substrate NH_4^+ -N, nitrification rates, *amoA*-AOA abundance, and product NO_3^- -N within the ENL. This coupled response demonstrates that the ENL is an actively responding biogeochemical reactor, rather than a passive recipient of leached NO_3^- -N. These results from the FSW-CZO demonstrate consistency with the first, second, and third ENL formation attributes (root-mediated transport, oxygenated microenvironments, and nitrifier communities), while emphasizing the fourth attribute (hydrological activation). Similar patterns were observed in the cropland-dominated Jiangnan Plain CZO⁴⁰, where rainfall drives subsoil NH_4^+ -N accumulation and ENL formation in the relatively high sand layer (Supplementary Fig. 13).

Together, the results from our case studies are consistent with the ENL formation pathways identified in the global analysis, corroborating the inferred nitrification mechanisms. While strong nitrification also occurs in the root zone (e.g., elevated *amoA*-AOA at -0.4 m depth; Fig. 3b), the exact depth of the ENL varies with local environmental conditions, as illustrated by the -0.7 m ENL in the FSW-CZO, and the -0.5 m ENL in the Jiangnan Plain CZO, both of which lie within the defined ENL depth interval (0.3–0.9 m). Our findings are derived primarily from intensively managed croplands in humid and sub-humid regions with neutral to acidic soils, as represented by two case study sites in southeastern China and central China, respectively. To test the generality of the ENL concept and develop region-specific management strategies, further experimentation is needed across a broader range of agricultural systems, including semi-arid to arid regions with alkaline soils, etc.

Implications for agroecosystem sustainability

The ENL constitutes a critical yet overlooked threat to agroecosystem sustainability by driving interconnected environmental degradation and N loss via two synergistic pathways: Firstly, the ENL accelerates the subsoil acidification trend (Fig. 5). Intensive N fertilization increases nitrification, a process that generates hydrogen ions^{29,39}, thereby driving soil acidification and ultimately reducing crop yields^{41,42}. Soil pH data (1961–2015, $n=104,759$) establish that a pervasive acidification trend in global cropland soils is significantly more acute within the ENL (ranging from 0.3 to 0.9 m), particularly at the depth of the TN peak (approximately 0.6 m) after the 1980s. This sharp and localized pH decline is strongly associated with soil TN content ($p < 0.01$). This finding highlights the urgent need for targeted management to alleviate acidification in this layer.

Secondly, the ENL acts as a biogeochemical engine for soil N leaching and groundwater NO_3^- -N pollution. We observed high NO_3^- -N (nitrification product) at the ENL depth, regardless of climate zone or crop root system length (Fig. 3b and Supplementary Fig. 10). However, below the ENL, both the sand content and the root distribution decline with soil depth (Fig. 3b and Supplementary Figs. 4 and 5), along with a decline in saturated soil hydraulic conductivity⁴³. These conditions will favor the production of NO_3^- -N from NH_4^+ -N after fertilizer applications in the ENL, and cause a consistent release of NO_3^- -N to groundwater. Our 3-year field observations at the FSW-CZO are consistent with this mechanism, showing a low NH_4^+ -N concentration in groundwater with no clear response to fertilization, but significantly high NO_3^- -N levels that exhibit a marked delayed response to fertilization (Supplementary Fig. 11). This demonstrates that the ENL intercepts and transforms most NH_4^+ -N into mobile NO_3^- -N, promoting ongoing NO_3^- -N leaching and groundwater contamination^{5-7,31,44}.

In the past decades, various cropland management practices have been employed to control nitrification, enhance N use efficiency, and minimize environmental pollution⁴⁵. Optimizing fertilizer rate, timing,

and placement at the soil surface remains the cornerstone of sustainable N management^{45,46}, as it directly reduces the overloaded N entering the subsoil system. However, a substantial fraction of residual N bypasses surface retention via root channels, preferential flow, or after sorption capacity is exceeded, and is transported to the subsurface, where it fuels the ENL. The identification of this biogeochemical engine thus addresses a long-standing ignored pathway, calling for an integrated two-pronged strategy: continued improvement of surface-based practices to minimize loading, combined with depth-specific interventions (e.g., targeted placement of nitrification inhibitors, irrigation scheduling to limit hydrological activation) that intercept N at the zone of peak transformation^{46,47}. Integrating both surface management and ENL-targeted interventions thus offers a more complete pathway for improving N use efficiency and safeguarding agroecosystem sustainability.

Methods

Global database

We integrated a comprehensive database of vertical soil N profiles from global croplands to explore the nitrification pattern. Our literature search on the Web of Science, using the keywords “cropland”, “agriculture”, “nitrogen”, “soil depth”, “soil profile”, and “vertical soil”, identified more than 2000 published papers (as of the end of 2022). Finally, a total of 107 papers were chosen according to three criteria: (i) the data on soil N originated from croplands; (ii) at least one variable related to soil N (TN, $\text{NH}_4^+\text{-N}$, $\text{NO}_3^-\text{-N}$) was reported in the paper; and (iii) the soil profiles were reported with at least two layers. In summary, we extracted 14 key data categories, including the first author, published year, country, longitude, latitude, soil depth, TN, $\text{NH}_4^+\text{-N}$, $\text{NO}_3^-\text{-N}$, *amoA*-AOA, *amoA*-AOB, mean annual precipitation, mean annual temperature, and crop type. Given that soil nitrification rates are typically low ($<0.1 \text{ mg kg}^{-1} \text{ d}^{-1}$) below 1 m depth^{48–51} and the global WTD distribution peak (2–7 m) limits oxygen supply^{29,37}, we collected soil N data from the 0–2 m depth. However, the hydrological and redox conditions in flooded paddy fields may limit nitrification²⁹. During our data collection, most studies only reported the dominant crop type, including paddy, making it difficult to accurately distinguish whether sampling was conducted during the fallow period or under flooded conditions. Therefore, our current data analysis includes both dryland and a small number of paddy systems. An analysis of the vertical patterns of soil nutrients excluding paddy systems is presented in Supplementary Fig. 7. The key patterns (including the subsurface peaks in TN, $\text{NH}_4^+\text{-N}$, $\text{NO}_3^-\text{-N}$, and *amoA*-AOA) remained consistent with those obtained using the full dataset, confirming the robustness of our findings. Detailed data and references are provided in Supplementary Tables 6 and 7, respectively.

Global distribution of plant MRD was derived from the Global Root Trait (GRooT) Database⁵². The vertical distribution of global soil TN, TOC, sand content, and pH was derived from the World Soil Information Service (WoSIS, December 2023) database (<https://www.isric.org/explore/wosis>). Global monthly soil moisture and temperature at depths of 0–0.1, 0.1–0.4, 0.4–1, and 1–2 m from 2010 to 2019 were collected from the Famine Early Warning Systems Network (FEWS NET) Land Data Assimilation System (FLDAS) products (FLDAS_NOAH01_C_GL_M; <https://disc.gsfc.nasa.gov/datasets>). Soil physicochemical properties data are classified into cropland and non-cropland (including forest, grassland, and shrubland) types based on the global distribution of land uses⁵³ at different periods (Supplementary Table 8). Soil inorganic N and sand content data were categorized according to the Köppen-Geiger climate classification (1980–2016)⁵⁴. Data regarding global agricultural N input were obtained from the FAOSTAT.

Fengpu stream watershed critical zone observatory (FSW-CZO)

Our FSW-CZO (117.2812°E, 24.3856°N) is located in the upper reaches of the West River of the Jiulong River, Fujian Province,

southeastern China (Supplementary Fig. 8). The FSW is an upper head watershed of the West River, which covers approximately 85 km², with regional elevation ranging from 49 to 999 m. The slope ranges from 0 to 71 degrees, and areas with a slope greater than 15 degrees account for 79%. This study area falls within a subtropical oceanic monsoon climate, with a mean annual temperature of 22.8 °C. The mean annual precipitation is 1,411 mm, mainly from March to September (wet season) with a high flow. The FSW is typically an agricultural watershed, primarily planted with pomelo, and covers 64% of the total area, with the rest as forest land (32%) and built-up land (4%).

Observation in the FSW-CZO

We conducted a three-year (2019–2021) monitoring of field management, hydro-meteorological conditions, and the dynamics of the soil and water environment in the FSW-CZO. Information on fertilization was collected based on detailed records of four farms in 2019. Since pomelo was the dominant industry in this region, there was no significant difference in field management between the years. The main stages of orchard management were summarized in Supplementary Fig. 9. Chemical fertilizer (diammonium phosphate, urea, and mixed fertilizer) and manure were the main nutrients to promote pomelo growth. The amount of fertilizer N was then converted based on the N content in each type of chemical fertilizer and manure used. Generally, approximately $1100 \pm 200 \text{ kg N ha}^{-1} \text{ yr}^{-1}$ was applied to the soils in FSW-CZO, which is significantly higher than the optimal N input ($150\text{--}250 \text{ kg ha}^{-1} \text{ yr}^{-1}$) in citrus orchards⁵⁵.

Soil samples were collected by depth at the entire watershed scale to explore the vertical pattern of soil texture in the FSW ($n = 2$, June 2019; $n = 14$, July 2020). Furthermore, to explore the seasonal variation in soil N, soil samples at different depths were collected at station S1 during the dry season ($n = 2$, November 2019 and January 2021) and the wet season ($n = 5$, August 2018, July 2019, March 2021, April 2021, and August 2021) using a portable impact drill-corer (Jujiang, Shandong, China). Because the WTD was mainly distributed at -1 m depth (Supplementary Table 2), a slightly greater depth (1.2 m) was considered for all soil sampling. The soil cores were divided at 0.2 m intervals. Here, the soils in both March and April of 2021 were further used to quantify the nitrification rate and microorganisms. Soil samples of -1 kg for each sample were placed on ice and transported to the laboratory for further analysis.

Soil water and groundwater were monitored at the outlet of the watershed (Supplementary Fig. 8). To explore the formation of ENL, soil water was monitored in three adjacent stations at a depth of 0.4–0.5 m (no water), 0.7–0.8 m ($n = 14$), and 1.1–1.2 m ($n = 34$) using ϕ 7 cm PVC pipes. The bottom of the pipes had 5 rows of ϕ 5 mm holes (0.1 m high), which were covered with a 0.1 mm nylon screen to allow the inflow of soil water. The pipes had a 0.5 m extension above the ground and were covered with a removable cap. Water samples were collected by a portable peristaltic pump on a monthly scale. Before sampling, the old water was drained to obtain freshwater samples. Adjacent to these pipes, a larger-diameter monitoring well (site #1) was installed in 2021 for real-time WTD measurements. Groundwater ($n = 278$) was sampled approximately every 4 days from 2019 to 2021 at a riparian well (-3 m depth, site #2) for nutrient analysis. A pressure transducer in this well-recorded real-time WTD from 2019 to 2020, supplemented by monthly manual measurements. To track groundwater N sources, monthly rainfall ($n = 7$) and groundwater ($n = 14$) samples for isotope analysis were collected from April 2020 to June 2021.

Hourly rainfall data were obtained from the National Meteorological Science Data Center (Pinghe weather station, <http://data.cma.cn/>). Hourly river flow data were provided by the local Hydrology and Water Resources Survey Sub-Center. These data were aggregated to daily or weekly scales as needed. Daily baseflow was estimated from daily river

flow using an automated separation procedure within the Hydrological Utility Package (<http://www.yibaipin.com/>).

Laboratory analysis

Soil $\text{NH}_4^+\text{-N}$ and $\text{NO}_3^-\text{-N}$ contents were measured by segmented flow automated colorimetry (San ++ analyzer, Germany) after extraction with 2 mol L^{-1} KCl. Soil particle size composition was determined by the Mastersizer 2000 particle size analyzer (Malvern Instruments, Malvern, UK). The soil gross nitrification rate was determined by the N isotope dilution method with $\delta^{15}\text{N-NO}_3^-$ additions⁵⁶. The gross nitrification rate was further multiplied by a coefficient of 0.76 (the proportion of autotrophic nitrification to gross nitrification) to represent the autotrophic nitrification rate²².

Soil genomic DNA was extracted using the E.Z.N.A. Soil DNA Kit (Omega Bio-Tek, Inc., USA). The extracted DNA was dissolved in 50 μL of TE buffer and stored at -20°C until analysis. DNA concentration was determined using a Nanodrop 2000 (Thermo Fisher Scientific, Inc., USA) for subsequent normalization in quantitative PCR (qPCR) assays. The abundance of N-cycle functional genes was quantified by qPCR using a Bio-Rad CFX96 system (Bio-Rad Laboratories, Inc., USA). Detailed qPCR conditions are provided in Supplementary Table 9.

Temperature, pH, dissolved oxygen (DO), and conductivity in the watershed water environment were measured using a WTW multi-parameter (Multi 3430, Germany). The contents of $\text{NH}_4^+\text{-N}$ and $\text{NO}_3^-\text{-N}$ in water samples were determined by segmented flow automated colorimetry (San ++ analyzer, Germany). Dual isotopes of nitrate ($\delta^{18}\text{O-NO}_3^-$ and $\delta^{15}\text{N-NO}_3^-$) were determined following a chemical reduction method⁵⁷. The detection of isotope samples was done by the Analytical Test Center of the Third Institute of Oceanography, Ministry of Natural Resources, China.

Statistical analysis

To obtain the lag time of groundwater N to fertilization, we first needed to determine N input at a daily scale. However, information on fertilization on a daily scale is largely unavailable in watersheds. Here, the annual fertilizer N was distributed on rainy days according to the proportion of weekly rainfall to annual total rainfall in fertilizing months (Supplementary Figs. 9 and 11a). This method was demonstrated to be optimal and consistent with agricultural practices in simulating the N output of the present study area⁵⁸. Here, both R^2 and the significance (p value) of linear regression were used to determine the lag time in the FSW-CZO. A t-test was used to compare differences in N and other parameters across seasons. Stable isotope analysis based on the SIAR model was used to calculate the contribution of major N sources from chemical fertilizer, manure and sewage, and rainfall to the groundwater $\text{NO}_3^-\text{-N}$. The ranges of $\delta^{15}\text{N-NO}_3^-$ and $\delta^{18}\text{O-NO}_3^-$ values of these sources and fractionation factors were shown in Supplementary Table 5.

Data availability

All data supporting the findings of this study are available within the article and the supplementary information files. Source data are provided with this paper.

References

- Wu, Y. et al. Policy distortions, farm size, and the overuse of agricultural chemicals in China. *Proc. Natl. Acad. Sci. USA* **115**, 7010–7015 (2018).
- Shahzad, A. N., Qureshi, M. K., Wakeel, A. & Misselbrook, T. Crop production in Pakistan and low nitrogen use efficiencies. *Nat. Sustain.* **2**, 1106–1114 (2019).
- Xu, P. et al. Fertilizer management for global ammonia emission reduction. *Nature* **626**, 792–798 (2024).
- Ludemann, C. I. et al. A global FAOSTAT reference database of cropland nutrient budgets and nutrient use efficiency (1961–2020): nitrogen, phosphorus and potassium. *Earth Syst. Sci. Data* **16**, 525–541 (2024).
- Ascott, M. J. et al. Global patterns of nitrate storage in the vadose zone. *Nat. Commun.* **8**, 1–7 (2017).
- Gu, B., Ge, Y., Chang, S. X., Luo, W. & Chang, J. Nitrate in groundwater of China: Sources and driving forces. *Global Environ. Chang.* **23**, 1112–1121 (2013).
- Liu, X. et al. Impact of groundwater nitrogen legacy on water quality. *Nat. Sustain.* **7**, 891–900 (2024).
- Yang, S. et al. Deep nitrate accumulation in a highly weathered subtropical critical zone depends on the regolith structure and planting year. *Environ. Sci. Technol.* **54**, 13739–13747 (2020).
- Brantley, S. L., Goldhaber, M. B. & Ragnarsdottir, K. V. Crossing disciplines and scales to understand the Critical Zone. *Elements* **3**, 307–314 (2007).
- Richter, D. D. & Mobley, M. L. Monitoring earth's critical zone. *Science* **326**, 1067–1068 (2009).
- Galloway, J. N. et al. Transformation of the nitrogen cycle: Recent trends, questions, and potential solutions. *Science* **320**, 889–892 (2008).
- Skiba, M. W., George, T. S., Baggs, E. M. & Daniell, T. J. Plant influence on nitrification. *Biochem. Soc. T.* **39**, 275–278 (2011).
- Zhang, K. et al. Inhibition of autotrophic nitrifiers in a nitrogen-rich paddy soil by elevated CO_2 . *Nat. Geosci.* **17**, 1254–1260 (2024).
- Guo, J. H. et al. Significant acidification in major Chinese croplands. *Science* **327**, 1008–1010 (2010).
- Yu, C. Q. et al. Managing nitrogen to restore water quality in China. *Nature* **567**, 516–520 (2019).
- Ho, J. C., Michalak, A. M. & Pahlevan, N. Widespread global increase in intense lake phytoplankton blooms since the 1980s. *Nature* **574**, 667–670 (2019).
- Dai, Y. et al. Coastal phytoplankton blooms expand and intensify in the 21st century. *Nature* **615**, 280–284 (2023).
- Van Meter, K. J., Van Cappellen, P. & Basu, N. B. Legacy nitrogen may prevent achievement of water quality goals in the Gulf of Mexico. *Science* **360**, 427–430 (2018).
- Carlson, K. M. et al. Greenhouse gas emissions intensity of global croplands. *Nat. Clim. Change* **7**, 63–68 (2016).
- Huang, Y. Y. et al. Size, distribution, and vulnerability of the global soil inorganic carbon. *Science* **384**, 233–239 (2024).
- Yang, Y. et al. Climate change exacerbates the environmental impacts of agriculture. *Science* **385**, 1058 (2024).
- Elrys, A. S. et al. Global gross nitrification rates are dominantly driven by soil carbon-to-nitrogen stoichiometry and total nitrogen. *Global Change Biol.* **27**, 6512–6524 (2021).
- Li, Z. et al. Global patterns and controlling factors of soil nitrification rate. *Global Change Biol.* **26**, 4147–4157 (2020).
- Zhang, Y. et al. Heterotrophic nitrification is the predominant NO_3^- production pathway in acid coniferous forest soil in subtropical China. *Biol. Fertil. Soils* **49**, 955–957 (2013).
- Macduff, J. H. & White, R. E. Net mineralization and nitrification rates in a clay soil measured and predicted in permanent grassland from soil-temperature and moisture-content. *Plant Soil* **86**, 151–172 (1985).
- Wild, B. et al. Microbial nitrogen dynamics in organic and mineral soil horizons along a latitudinal transect in western Siberia. *Global Biogeochem. Cycles* **29**, 567–582 (2015).
- Lu, X. D., Nicol, G. W. & Neufeld, J. D. Differential responses of soil ammonia-oxidizing archaea and bacteria to temperature and depth under two different land uses. *Soil Biol. Biochem.* **120**, 272–282 (2018).
- Lyu, C. et al. Insight into the microbial nitrogen cycle in riparian soils in an agricultural region. *Environ. Res.* **231**, 116100 (2023).

29. Xin, J. et al. The missing nitrogen pieces: A critical review on the distribution, transformation, and budget of nitrogen in the vadose zone-groundwater system. *Water Res.* **165**, 114977 (2019).
30. Fan, Y., Miguez-Macho, G., Jobbagy, E. G., Jackson, R. B. & Otero-Casal, C. Hydrologic regulation of plant rooting depth. *Proc. Natl. Acad. Sci. USA.* **114**, 10572–10577 (2017).
31. Zhu, Q., Castellano, M. J. & Yang, G. Changes in soil carbon and nitrogen stocks and microbial community after forest conversion in a subtropical region. *Scand. J. Forest Res.* **36**, 575–584 (2021).
32. Zhang, S., Huffman, T., Zhang, X., Liu, W. & Liu, Z. Spatial distribution of soil nutrient at depth in black soil of Northeast China: a case study of soil available phosphorus and total phosphorus. *J. Soil. Sediment.* **14**, 1775–1789 (2014).
33. Elrys, A. S. et al. Patterns and drivers of global gross nitrogen mineralization in soils. *Global Change Biol.* **27**, 5950–5962 (2021).
34. Du, Y., Guo, S., Wang, R., Song, X. & Ju, X. Soil pore structure mediates the effects of soil oxygen on the dynamics of greenhouse gases during wetting-drying phases. *Sci. Total Environ.* **895**, 165192 (2023).
35. Gramlich, A., Stoll, S., Stamm, C., Walter, T. & Prasuhn, V. Effects of artificial land drainage on hydrology, nutrient and pesticide fluxes from agricultural fields: A review. *Agr. Ecosyst. Environ.* **266**, 84–99 (2018).
36. Guan, Y. et al. Anthropogenic enhancement of subsurface soil moisture droughts. *Nat. Clim. Chang.* **15**, 1355–1362 (2025).
37. Fan, Y., Li, H. & Miguez-Macho, G. Global patterns of groundwater table depth. *Science* **339**, 940–943 (2013).
38. Jasechko, S. et al. Rapid groundwater decline and some cases of recovery in aquifers globally. *Nature* **625**, 715–721 (2024).
39. Li, Y., Chapman, S. J., Nicol, G. W. & Yao, H. Nitrification and nitrifiers in acidic soils. *Soil Biol. Biochem.* **116**, 290–301 (2018).
40. Zhang, L. et al. Influence of seasonal water-level fluctuations on depth-dependent microbial nitrogen transformation and greenhouse gas fluxes in the riparian zone. *J. Hydrol.* **620**, 129457 (2023).
41. Dai, Z. et al. Long-term nitrogen fertilization decreases bacterial diversity and favors the growth of Actinobacteria and Proteobacteria in agro-ecosystems across the globe. *Global Change Biol.* **24**, 3452–3461 (2018).
42. Zhang, W. et al. Stabilization of acidification in China's cropland soils. *Nat. Geosci.* **18**, 1125–1132 (2025).
43. Gupta, S., Hengl, T., Lehmann, P., Bonetti, S. & Or, D. SoilKsatDB: global database of soil saturated hydraulic conductivity measurements for geoscience applications. *Earth Syst. Sci. Data* **13**, 1593–1612 (2021).
44. Almaraz, M., Wang, C. & Wong, M. Y. Deep soil contributions to global nitrogen budgets. *Nat. Commun.* **16**, 966 (2025).
45. Gu, B. et al. Cost-effective mitigation of nitrogen pollution from global croplands. *Nature* **613**, 77–84 (2023).
46. Elrys, A. S. et al. Integrative knowledge-based nitrogen management practices can provide positive effects on ecosystem nitrogen retention. *Nat. Food* **4**, 1075–1089 (2023).
47. Lam, S. K. et al. Next-generation enhanced-efficiency fertilizers for sustained food security. *Nat. Food* **3**, 575–580 (2022).
48. Khalili, B. & Nourbakhsh, F. Vertical distribution of soluble organic nitrogen, nitrogen mineralization, nitrification, and amidohydrolase activities in a manure-treated soil. *J. Plant Nutr. Soil Sc.* **175**, 265–272 (2011).
49. Wang, Y., Ji, H., Wang, R., Hu, Y. & Guo, S. Synthetic fertilizer increases denitrifier abundance and depletes subsoil total nitrogen in a long-term fertilization experiment. *Front. Microbiol.* **11**, 1–11 (2020).
50. Wang, J. et al. Ammonia oxidizer abundance in paddy soil profile with different fertilizer regimes. *Appl. Soil Ecol.* **84**, 38–44 (2014).
51. Li, Y., Xu, C., Wang, S. & Wang, Y. Modelling nitrogen transport and transformation in a transplanted rice field experiment with reduced irrigation. *Acta Agri. Scand. B-S P.* **68**, 457–470 (2018).
52. Guerrero-Ramírez, N. R. et al. Global root traits (GRooT) database. *Glob. Ecol. Biogeogr.* **30**, 25–37 (2020).
53. Liu, H. et al. Annual dynamics of global land cover and its long-term changes from 1982 to 2015. *Earth Syst. Sci. Data* **12**, 1217–1243 (2020).
54. Beck, H. E. et al. Present and future Koppen-Geiger climate classification maps at 1-km resolution. *Sci. Data* **5**, 180214 (2018).
55. Qin, W., Assinck, F. B. T., Heinen, M. & Oenema, O. Water and nitrogen use efficiencies in citrus production: A meta-analysis. *Agr. Ecosyst. Environ.* **222**, 103–111 (2016).
56. Wang, F. et al. Saltmarsh sediments with wastewater input emit more carbon greenhouse gases but less N₂O than mangrove sediments. *Catena* **213**, 106205 (2022).
57. McIlvin, M. R. & Altabet, M. A. Chemical conversion of nitrate and nitrite to nitrous oxide for nitrogen and oxygen isotopic analysis in freshwater and seawater. *Anal. Chem.* **77**, 5589–5595 (2005).
58. Xiong, R. et al. Predicting dynamic riverine nitrogen export in unmonitored watersheds: Leveraging insights of AI from data-rich regions. *Environ. Sci. Technol.* **56**, 10530–10542 (2022).

Acknowledgements

This research was primarily supported by the National Natural Science Foundation of China (No. 42530405, No. 42322901, and No. 51961125203), with partial support from the Hong Kong General Research Fund (No. 17307521 and No. C7082-22GF), and the Fujian Province Water Conservancy Science and Technology Project (No. MSK202301 and No. MSK202313). We thank Prof. Susan L. Brantley from Pennsylvania State University and Prof. Scott Jasechko from the University of California for their insightful comments. We thank Mingfa Zhu, Yan Fang, Ailin Yang, Junou Du, Junxian Pei, Dapeng Huang's team, and the local villagers for their assistance in lab analysis and fieldwork.

Author contributions

Y.W., X.L., and N.C. conceptualized the study. Y.W., Y.Y., F.W., Z.L., and R.Y. performed the field investigation. Y.W. collected and analyzed the data, prepared the figures, and drafted the original manuscript. X.L., E.G.J., N.B.B., G.Z., Y.Z., B.G., S.Z., S.X.C., Y.L., and N.C. substantially contributed to the manuscript development. N.C. and X.L. secured the funds.

Competing interests

The authors declare no competing interests.

Additional information

Supplementary information The online version contains supplementary material available at <https://doi.org/10.1038/s41467-026-70277-7>.

Correspondence and requests for materials should be addressed to Xin Luo or Nengwang Chen.

Peer review information *Nature Communications* thanks Jeanette Norton and the other, anonymous, reviewer(s) for their contribution to the peer review of this work. A peer review file is available.

Reprints and permissions information is available at <http://www.nature.com/reprints>

Publisher's note Springer Nature remains neutral with regard to jurisdictional claims in published maps and institutional affiliations.

Open Access This article is licensed under a Creative Commons Attribution-NonCommercial-NoDerivatives 4.0 International License, which permits any non-commercial use, sharing, distribution and reproduction in any medium or format, as long as you give appropriate credit to the original author(s) and the source, provide a link to the Creative Commons licence, and indicate if you modified the licensed material. You do not have permission under this licence to share adapted material derived from this article or parts of it. The images or other third party material in this article are included in the article's Creative Commons licence, unless indicated otherwise in a credit line to the material. If material is not included in the article's Creative Commons licence and your intended use is not permitted by statutory regulation or exceeds the permitted use, you will need to obtain permission directly from the copyright holder. To view a copy of this licence, visit <http://creativecommons.org/licenses/by-nc-nd/4.0/>.

© The Author(s) 2026